One-way transmission of electrons on the topological insulator surface modulated by magnetic potential

Jin-Jing Li, Rui-Li Zhang, Han-Tian Gao, Ru-Wen Peng, R. S. Huang, and Mu Wang

Citation: Journal of Applied Physics **122**, 214301 (2017);
View online: https://doi.org/10.1063/1.5002728
View Table of Contents: http://aip.scitation.org/toc/jap/122/21
Published by the American Institute of Physics

One-way transmission of electrons on the topological insulator surface modulated by magnetic potential

Jin-Jing Li, Rui-Li Zhang,[a] Han-Tian Gao, Ru-Wen Peng,[a] R. S. Huang, and Mu Wang
National Laboratory of Solid State Microstructures, School of Physics, and Collaborative Innovation Center of Advanced Microstructures, Nanjing University, Nanjing 210093, China

(Received 1 September 2017; accepted 15 November 2017; published online 7 December 2017)

We investigate the transport properties of Dirac fermions on the surface of a three-dimensional topological insulator (TI) with magnetic modulation potentials. By using the transfer-matrix method, the transmission coefficients are obtained as a function of incident energy and incident angle. It is shown that the forward and backward propagating carriers possess different transmission coefficients at some incident energies when the charge carriers incident obliquely, which originates from the break of time reversal symmetry. Particularly, the magnetic barrier introduces asymmetric scattering; thus, the scattered angles are different for the forward and backward propagating carriers. As a consequence, the transmission in one direction is permitted while it is blocked in its reversal direction. Therefore, the unidirectional transmission of electrons is achieved on the surface of TI. Furthermore, unidirectional transmission is demonstrated by the electronic charge distributions in the system. The investigations may have potential applications in the design of TI-based one-way quantum devices. *Published by AIP Publishing.* https://doi.org/10.1063/1.5002728

I. INTRODUCTION

In recent years, topological insulator (TI) has become one of the most intensively studied systems in condensed matter physics and material science.[1–5] TI is an unusual quantum state of matter which is distinguished from a normal band insulator by a nontrivial topological invariant Z_2 characterizing its band structure.[6–8] In TIs, there exist a bulk energy gap and gapless edge or surface states residing in the bulk gap in the absence of magnetic fields.[6–9] The existence of edge and surface states has been confirmed by an experiment in HgTe quantum wells,[10] and angle-resolved photoemission spectroscopy experiments in three-dimensional (3D) Bi_2Se_3,[11] Bi_2Te_3,[12] and Sb_2Te_3,[13] respectively. It is demonstrated that the surface states of TIs exhibit Dirac cone-shaped conduction and valence bands that meet at the Γ point.[11–13] Unlike conventional two-dimensional (2D) electron states, these surface states are robust against the disorder scattering and electron–electron interactions due to the protection by the time reversal symmetry.[14] Therefore, researchers are motivated to consider whether some electronic devices with strong anti-interference and low power consumption could be fabricated based on TIs.

To realize the practical TI-based devices, it is essential to develop some means of controlling or modifying their surface states. The strategies of quantum confinement,[15] depositing ferromagnetic insulating strips,[16] decorating with magnetic adatoms,[17] and applying a gate voltage[18] on the top of the TI surface have been used to achieve this goal. By decorating Mn adatoms, Narayan *et al.* demonstrated a single atom anisotropic magnetoresistance on the surface of a TI.[17] Their results reveal the real space spin texture around the magnetic impurity and lead to a proposed device set-up for experimental realization. On the other hand, by coating the magnetic or superconducting layers on TIs, the surface states could be gapped and many interesting properties arise, such as the half-integer quantum Hall effect[19] and Majorana fermions.[20] Recently, Wu *et al.* demonstrated a directional-dependent tunneling of electrons on the surface of a TI[21] with magnetic barriers. By using the magnetic barriers, the time-reversal symmetry is broken, and thus, the transport properties of surface states on a TI are modified. In semiconductors, an example associated with the breaking of time-reversal symmetry is the nonreciprocal response of electrons, i.e., the electrical diode. Stimulated by the vast application of electrical diode, considerable efforts have been dedicated to the study of nonreciprocal propagation of light.[22] Afterwards, a non-reciprocal propagation of terahertz waves through a photonic crystal cavity integrated with graphene is achieved under an external magnetic field.[23]

In this work, we study the unidirectional transmission of Dirac fermions on the surface of a 3D TI with magnetic barriers. The magnetic barrier introduces an asymmetric scattering, and thus, the scattered angles are different for the forward and backward propagating carriers. As a consequence, a unidirectional transmission is achieved on the surface of a 3D TI, which has been verified by the transmission spectra and the electronic charge distributions. Furthermore, by tuning the periodicity of the system, such a unidirectional transmission can be drastically tuned. This tunable unidirectional transmission may have potential applications in the design of TI-based devices, which can let a specific mode pass, but its time reversal counterpart stops.

II. THE THEORETICAL MODEL

Consider the behavior of charge carriers on the surface of a TI with magnetic potentials. The magnetic potentials

[a]Authors to whom correspondence should be addressed: rlzhang@nju.edu.cn and rwpeng@nju.edu.cn

can be created underneath ferromagnetic insulator (FI) strips via a magnetic proximity effect.[24] Suppose that the FI strips are deposited on the surface of TI (i.e., x-y plane) with the interfaces between FI and TI paralleling to the y-axis (as shown in Fig. 1). We designate the regions with and without FI strips as A and B, respectively, and they are distributed as $R(m) = (\mathrm{AB})^m(\mathrm{BA})^m$ [Fig. 1(a)]. The width of region A is set as d_A, and the distance between the two FI strips is d_B, and we fixed the width $d_A = d_B = d$. The magnetization of the ferromagnetic stripe can be perpendicular or parallel to the surface of the TI. Correspondingly, the square-shaped and delta-function-shaped magnetic fields can be created, respectively.[24] In all cases, the magnetic fields can break the time reversal symmetry of the system, and the unidirectional transmission can happen. In this work, we focus on the delta-function-shaped magnetic field, $B_z(x) = B\delta(x)$, perpendicular to the surface of the TI at the boundary of the strip [Fig. 1(a)]. Such magnetic field profiles approximate those realized by depositing Co micro-magnetic strips on the top of the two-dimensional electron gas.[25] Then, a magnetic vector step is created which can be written as $A_y(x) = A_y\theta(x)$. Here, we have adopted Landau gauge $A = [0, A_y(x), 0]$. Then, the effective Hamiltonian of the low-energy electrons near the Γ point of the Dirac cones can be written as

$$H = v_F\sigma \cdot (\pi \times \hat{z}) + H_Z + V, \tag{1}$$

where $\sigma = (\sigma_x, \sigma_y, \sigma_z)$ are the Pauli matrices, and the Fermi velocity is $v_F = 5 \times 10^5$ m/s corresponding to the material of Bi_2Se_3. $\pi = p + eA$ is the momentum with vector potential A generated by the FI strips, and $\hat{z}$ is the unit vector normal to the surface. The term $H_Z = g\mu_B\sigma \cdot B$ is induced by the Zeeman spin spitting, which can be negligible at a low magnetic field.

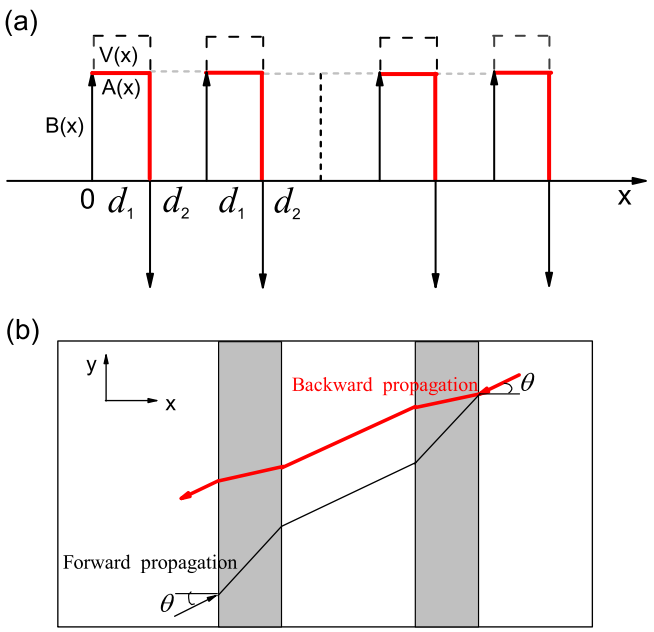

FIG. 1. (a) Profiles of the symmetric potentials distributed as $R(m) = (\mathrm{AB})^m(\mathrm{BA})^m$. (b) Profiles of electron scattering of the system: the black and red arrows represent FP and BP, respectively. d_A and d_B are the width of the regions with and without magnetic barriers, respectively, and θ is the incident angle of carriers.

In order to simplify the notation, we introduce the dimensionless length and energy units: $l_B = (\hbar/eB_0)^{1/2}$, $E_0 = \hbar v_F/l_B$, as well as $A_y(x) \to B_0 l_B A_y(x)$, $E \to E_0 E$, $V \to E_0 V$, $r \to l_B r$, $k \to k/l_B$, and the Hamiltonian becomes

$$H = \begin{pmatrix} g\mu_B B + V & k_y + A_y + ik_x \\ k_y + A_y - ik_x & -g\mu_B B + V \end{pmatrix}. \tag{2}$$

This Hamiltonian acts on a state expressed by a two-component wavefunction $\Psi = (\psi_1, \psi_2)^T$. Due to the translational invariance of the system along the y-direction, the wavefunction $\psi_{1,2}$ can be written as $\psi_{1,2}(x, y) = \psi_{1,2}(x)e^{ip_{\mathrm{A,B}}y}$ with $p_\mathrm{A} = k_y + A_y$ in region A (with modulation potentials), and $p_B = k_y$ in region B (without modulation potentials). At the input and output side of the regions A, the wavefuntions have the relation of

$$\begin{pmatrix} \psi_1(x + d_A) \\ \psi_2(x + d_A) \end{pmatrix} = M_A \begin{pmatrix} \psi_1(x) \\ \psi_2(x) \end{pmatrix}, \tag{3}$$

where the transfer matrix M_A is obtained as

$$M_A = \frac{1}{\cos\phi_A} \begin{pmatrix} \cos(q_A d_A - \phi_A) & -\sin(q_A d_A) \\ \sin(q_A d_A) & \cos(q_A d_A + \phi_A) \end{pmatrix}. \tag{4}$$

Here, $\phi_A = \arcsin(p_A/k_A)$ denotes the refraction angle of carriers inside the region A, and $k_A = (E - V)/\hbar v_F$ is the wave vector of incident carriers with energy E. The x component of k_A can be expressed as $q_A = sign(k_A)\sqrt{k_A^2 - p_A^2}$ for $p_A^2 < k_A^2$, otherwise $q_A = i\sqrt{p_A^2 - k_A^2}$. When the carriers transport across the region B, the transfer matrix M_B has the same form as Eq. (4) by replacing the subscript A with B. Therefore, we can get the total transfer matrix M across the system, relating the incident and reflection waves to the transmission wave. Then, the electronic transmission coefficient T can be obtained as

$$T = \left| \frac{2i\cos\theta_i}{i(M_{22}e^{-i\theta_i} + M_{11}e^{i\theta_e}) - M_{12}e^{i(\theta_e - \theta_i)} + M_{21}} \right|^2, \tag{5}$$

where $\theta_i(\theta_e)$ is the angle between the incident (exit) direction of carriers and the x-axis at the input (output) side of the system, and $M_{ij}(i, j = 1, 2)$ is the matrix element of the total transfer matrix M.

It should be noted that the angle $\phi_A = \arcsin(p_A/k_A)$ in the region A is different for the forward and backward propagating carriers when the carriers incident obliquely (i.e., $k_y \neq 0$). Specifically, the angle is $\phi_A = \arcsin[(k_y + A_y)/k_A]$ for the forward transmission, while it is $\phi_A = \arcsin[(-k_y + A_y)/k_A]$ for the backward transmission. This indicates that the incident carriers cannot return to their original point of incidence because of the magnetic modulation potential. On the other hand, the transfer matrix M_A is changed for the backward transmission compared with that for the forward transmission when the carriers incident with a nonzero angle. Then, the transmission coefficient will be different for the forward and backward propagating carriers. This feature provides a possibility of unidirectional transmission. Physically,

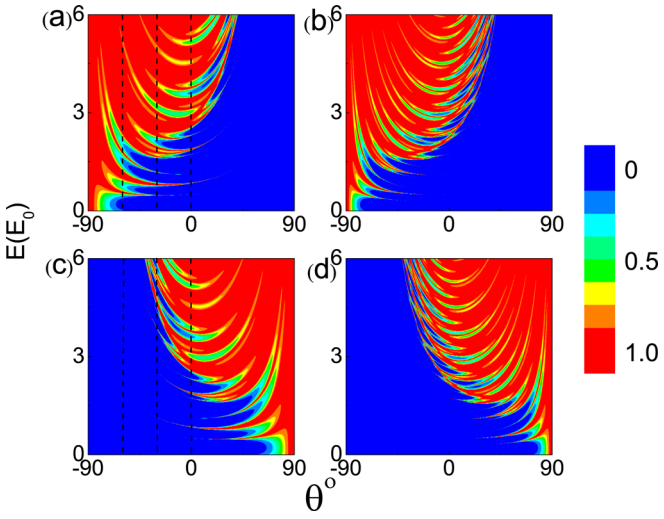

FIG. 2. The contour plot of transmission coefficients as functions of incident angle θ and energy E in the system with $m = 2$ when $B = 1$, $V = 1$, $E_0 = 16\,\text{meV}$, and $l_B = 26\,\text{nm}$ for the FP: (a) $d_A = d_B = 2$; (b) $d_A = d_B = 4$; and for BP: (c) $d_A = d_B = 2$; (d) $d_A = d_B = 4$. The vertical dashed lines are the guide lines presenting different incident angles.

the magnetic modulation potentials break the time-reversal symmetry, and the unidirectional transmission of electrons is obtained on the surface of a TI.

III. THE NUMERICAL CALCULATIONS

Based on the above analysis, we numerically investigate the quantum transport on the surface of a TI with delta-function-shaped magnetic barriers distributed as $R(m) = (\text{AB})^m(\text{BA})^m$. Let us take the system with two unit cells (i.e., $m = 2$) as an example. First, we present the transmission coefficients as functions of incident energy and incident angle when the charge carriers incident from left to right [forward propagation (FP)] through the system with different widths d of FI strips [Figs. 2(a) and 2(b)]. It is shown in Fig. 2(a) that the contour plot of transmission coefficients demonstrates an asymmetric distribution with respect to the axis of $\theta = 0^\circ$ (i.e., the normal incident direction). By fixing the incident energy, the transmission coefficients at different angles are different. Thus, the magnetic barriers lead to an anisotropic propagation of charge carriers. When the width d of the magnetic barriers is increased, the continuous range of red color with larger transmission coefficients is reduced by "inserting" small gaps [Fig. 2(b)]. Second, we demonstrate the transmission spectra in Figs. 2(c) and 2(d) when the charge carrier incident from right to left [backward propagation (BP)] through the system corresponding to Figs. 2(a) and 2(b), respectively. Similarly, the contour plot of transmission spectra is asymmetric with respect to axis of $\theta = 0^\circ$ (i.e., the normal incident direction) for the backward propagation [Fig. 2(c)]. When the width of the magnetic barriers is increased, more transmission gaps appear between the regions of red color, which denotes larger transmission coefficients [Fig. 2(d)]. Interestingly, the contour plot of transmission spectra for the backward propagation (BP) is different from that for the forward propagation (FP) [Figs. 2(a) versus 2(c), and 2(b) versus 2(d)]. For certain incident energy and incident angle, the transmission peaks appear for the FP while the transmission coefficients are zero for the BP. Therefore, the unidirectional transmission of electrons is obtained on the surface of a TI by applying magnetic barriers.

It is worthwhile to focus on some specific incident angles and compare FP with BP. As examples, we draw three vertical lines in Figs. 2(b) and 2(d), which correspond to $\theta = 0^\circ$, -30°, and -60°, respectively. It is found that the transmission spectra for the FP and BP coincide with each other when $\theta = 0^\circ$ [Fig. 3(a)]. However, they are uncoupled when the incidence is oblique with $\theta = -30^\circ$ and -60° [Figs. 3(b) and 3(c)]. At some incident energies, the transmission coefficients are one for the FP while the transmission coefficients are zero for the BP. This feature originates from the asymmetric scattering of the magnetic barriers, which lead to the difference of the refraction angles for the

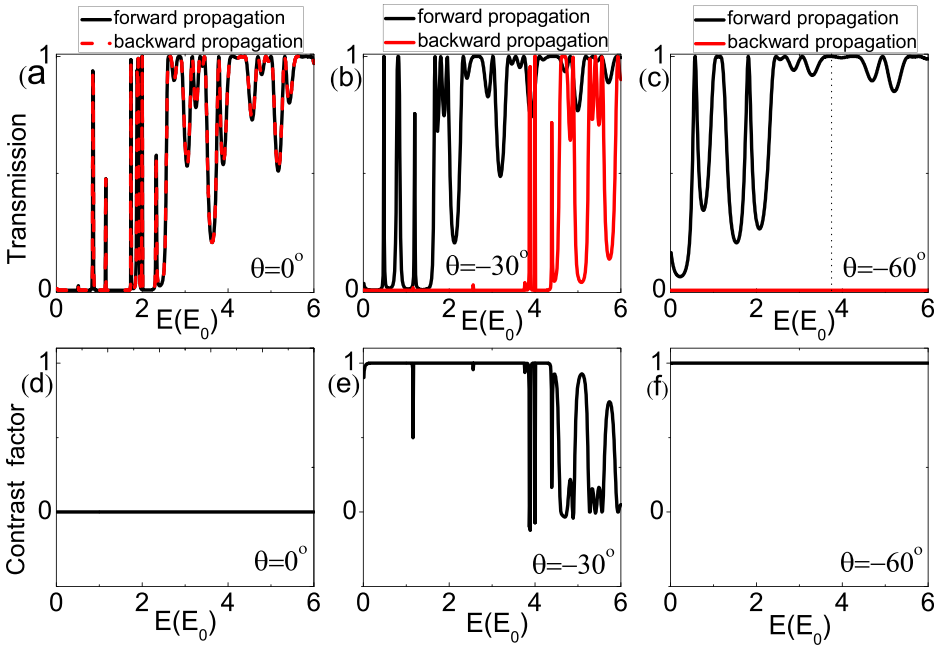

FIG. 3. (a), (b), and (c) present the transmission coefficients T versus the incident energy E in the system with $d_A = d_B = 2$, $m = 2$, $B = 1$, $V = 1$, $E_0 = 16\,\text{meV}$, $l_B = 26\,\text{nm}$, and different incident angles: (a) $\theta = 0^\circ$; (b) $\theta = -30^\circ$; (c) $\theta = -60^\circ$. The black and red lines represent FP and BP, respectively. (d), (e), and (f) plot the Contrast factor against the incident energy E in the system corresponding to (a), (b), and (c), respectively.

FP and BP. As a consequence, the transfer matrix M_A is changed for the BP compared with that for the FP when the carriers incident obliquely. Then, the transmission coefficient will be different for the FP and BP. Physically, the magnetic modulation potentials break the time-reversal symmetry, and the transmission in one direction is permitted while it is blocked in its reversal direction. In order to measure the asymmetry quantificationally, we define a Contrast factor $C = (T_f - T_b)/(T_f + T_b)$ where T_f and T_b indicate the transmission coefficients for the forward and backward propagating charge carriers, respectively. Obviously, C equals to zero if the same transmission coefficient is achieved for both the FP and BP. However, C equals to ± 1 if the transmission of one direction is completely blocked. Figures 3(d)–3(f) plot the Contrast factors as a function of incident energy with different incident angles θ. For $\theta = 0^\circ$, i.e., the normal incidence, there exists no unidirectional propagation where the contrast factor is zero [Fig. 3(d)]. For the oblique incidence with $\theta = -30^\circ$, there exists unidirectional propagation where the contrast factor reaches its maximum [Fig. 3(e)]. By increasing the incident angles, more backward propagating modes are blocked. Thus, a tunable unidirectional transmission can be obtained and optimized on the surface of TI with magnetic barriers. These properties may be used in the design of TI-based one-way quantum devises.

Quantum transport on the surface of TI with magnetic barriers will be influenced by the number of the period. Figures 4(a) and 4(b) show the transmission spectra for the FP and BP, respectively, when $d = 2$, and the number of period is $m = 6$. It is evident that more gaps appear in the transmission spectra compared with that for $m = 2$ [Fig. 2(a)]. In general, by increasing the number of cells, more and more transmission zones diminish gradually and some of them approach zero transmission. Therefore, a distinct bandgap structure appears in the system. On the other hand, the transmission spectra do not coincide with each other for the FP and BP [Figs. 4(a) and 4(b)]. If we fix the incident angles as $\theta = 0^\circ$ and -30°, respectively, the corresponding transmission coefficients against the incident energy are present in Figs. 4(c) and 4(d). Obviously, the oscillating behavior of transmission becomes more significant as the number of unit cells is increased due to the multiple scattering. For the normal incidence with $\theta = 0^\circ$, the transmission spectra for the FP and BP coincide with each other [Fig. 4(c)]. For the oblique incidence with $\theta = -30^\circ$, the transmission spectra are separated for the FP and BP [Fig. 4(d)]. It is noted that the transmissivity of BP is weakened by increasing the number of the unit cells. This feature provides another way of optimizing the unidirectional transmission. Therefore, the unidirectional transmission is kept and optimized when the number of the unit cells is increased.

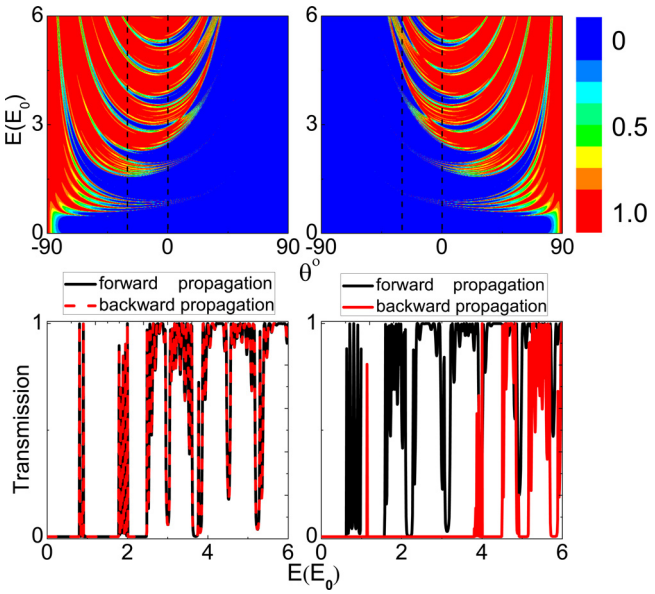

FIG. 4. (a) and (b) show the contour plot of transmission coefficients against the incident angle θ and energy E for the FP and BP, respectively, in the system with $d_A = d_B = 2$, and $m = 6$ when $B = 1$, $V = 1$, $E_0 = 16$ meV, and $l_B = 26$ nm. The vertical dashed lines are the guide lines presenting different incident angles. (c) and (d) depict the transmission coefficients T versus the incident energy E in the system corresponding to (a) and (b), respectively, and incident angles: (c) $\theta = 0^\circ$; (d) $\theta = -30^\circ$. The black and red lines represent FP and BP, respectively.

In order to clearly understand the unidirectional transmission of charge carriers on the surface of TI with magnetic barriers, the charge distributions have been studied. At arbitrary point along the x-axis of the system, the charge density is determined by $|\Psi(x)|^2$. We calculated the charge distributions by using the continuous boundary conditions and the limitation that the summation of transmission coefficient T and reflection coefficient R is unit. Figures 5(a) and 5(b) plot the charge distributions for the FP and BP in the system with $m = 2$, $d_A = d_B = 2$, $B = 1$, $V = 1$, $E = 3.7$, and $\theta = -60^\circ$. It is demonstrated that the charge distribution possesses almost an equal amplitude along the system for the FP [Fig. 5(a)]. That implies that the incident wave is extended in the whole system. Then, the FP is allowed. However, the charge distributions decay exponentially along the system [Fig. 5(b)] for the BP. This indicates that the incident wave is localized in the system, and the BP is forbidden. Particularly, there is a transmission peak for the FP, and the transmission coefficient is zero for the BP in the system when the incident energy and incident angle are $E = 3.7$ and $\theta = -60^\circ$, respectively [Fig. 3(c)]. On the other hand, the charge distributions

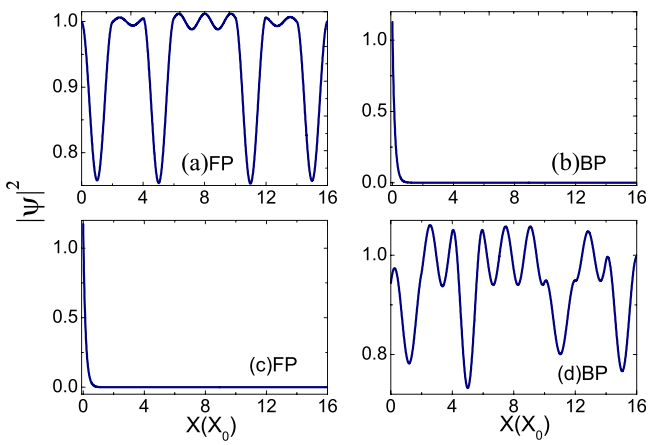

FIG. 5. The charge distributions in the system with $d_A = d_B = 2$, $m = 2$, and the unit of length $X_0 = l_B = 26$ nm when $B = 1$, $V = 1$, and $E_0 = 16$ meV. (a) FP and (b) BP with $E = 3.7$ and $\theta = -60^\circ$, respectively. (c) FP and (d) BP with $E = 3.9$ and $\theta = 60^\circ$, respectively.

at the energy $E = 3.9$ and the incident angle $\theta = 60^\circ$ are also presented for the FP and BP in Figs. 5(c) and 5(d), respectively. In this case, the charge distributions exponentially decay for FP while it is extended for BP, which correspond to the zero transmissivity for FP [Fig. 2(a)] and transmission peak for BP [Fig. 2(c)], respectively. All these electronic states indeed determine the quantum transport in the system. This implies that, by applying magnetic barriers on the surface of TI, unidirectional transmission can be achieved which may be applied in the design of TI-based one-way quantum devices.

It is worthwhile to mention several aspects that may arise in the real systems. (i) In some TIs, such as Bi_2Te_3, the surface states can have a hexagonal warping in the dispersion. Then, the Hamiltonian can be written as $H = v(k_x\sigma_y - k_y\sigma_x) + \lambda\sigma_z(k_x^3 - 3k_xk_y^2)$.[26] By considering the hexagonal warping, the transmission spectra will be modified, but the unidirectional character may be kept. The reason is that, by applying a magnetic field as depicted in our manuscript, the scattered angles are different for the forward and backward propagating carriers when the carriers incident obliquely (i.e., $k_y \neq 0$). Further investigations will be undertaken. (ii) For the finite-temperature transport in TIs, electron-phonon scattering is an important scattering mechanism.[27] Therefore, the finite temperature is to suppress the conductivity while the unidirectional character should be still maintained. (iii) The transport signature of surface states will be reduced by considering the bulk conductance. Fortunately, recent experimental advances in materials preparation and thin film device fabrication have made it possible to see the expected pure 2D surface conduction with little contamination from the bulk states.[28] In our work, we concentrated entirely on the 2D surface states and ignored the complications of the bulk conduction and the bulk carriers which should not alter the unidirectional character. (iv) Depositing ferromagnetic insulator strips on the TI surface may also induce electrostatic effects, such as Rashba-type spin-orbit coupling (SOC). It is shown that the spin helicities of the TI surface states and the Rashba-type SOC are opposite.[29] Li *et al.* directly compared the electrical measurements of spin polarization in Bi_2Se_3 with the potential coexistence of both Dirac and trivial Rashba surface states and InAs with only the Rashba states. They show that the spin voltages measured for the Dirac and Rashba systems are indeed opposite in sign. However, the dominant contribution in the TI is from the Dirac surface states.[30] Therefore, in our work, the unidirectional transmission is still possible by considering the Rashba-type SOC, although it may weaken the signals.

IV. SUMMARY

By using the transfer-matrix method, the transmission spectra of Dirac fermions on the surface of a three-dimensional topological insulator with magnetic modulation potentials are obtained. It is found that the transmission in one direction is permitted while it is blocked in its reversal direction due to the break of time reversal symmetry. Then, the unidirectional transmission of electrons is obtained on the surface of TI with magnetic barriers. Furthermore, the character of unidirectional transmission is demonstrated by the electronic charge distributions in the system. The strong dependence of transmission on the direction gives the possibility to construct TI-based one-way quantum devices.

ACKNOWLEDGMENTS

This work was supported by grants from the National Natural Science Foundation of China (Grant Nos. 10904061, 11634005, 61475070, 11474157, 11674155, and 11621091), the State Key Program for Basic Research from the Ministry of Science and Technology of China (Grant Nos. 2017YFA0303702 and 2014CB921103), and China Scholarship Council.

[1]J. E. Moore, Nature **464**, 194 (2010).
[2]X. L. Qi and S. C. Zhang, Rev. Mod. Phys. **83**, 1057 (2011).
[3]Z. F. Wang, Z. Liu, and F. Liu, Phys. Rev. Lett. **110**, 196801 (2013).
[4]Y. Ma, L. Kou, Y. Dai, and T. Heine, Phys. Rev. B **94**, 201104(R) (2016).
[5]S. Manna, A. Kamlapure, L. Cornils, T. Hänke, E. M. J. Hedegaard, M. Bremholm, B. B. Iversen, P. Hofmann, J. Wiebe, and R. Wiesendanger, Nat. Commun. **8**, 14074 (2017).
[6]C. L. Kane and E. J. Mele, Phys. Rev. Lett. **95**, 146802 (2005).
[7]L. Fu, C. L. Kane, and E. J. Mele, Phys. Rev. Lett. **98**, 106803 (2007).
[8]L. Fu and C. L. Kane, Phys. Rev. B **76**, 045302 (2007).
[9]M. Z. Hasan and C. L. Cane, Rev. Mod. Phys. **82**, 3045 (2010).
[10]M. König, S. Wiedmann, C. Brüne, A. Roth, H. Buhmann, L. W. Molenkamp, X. L. Qi, and S. C. Zhang, Science **318**, 766 (2007).
[11]Y. Xia, D. Qian, D. Hsieh, L. Wray, A. Pal, H. Lin, A. Bansil, D. Grauer, Y. S. Hor, R. J. Cava, and M. Z. Hasan, Nat. Phys. **5**, 398 (2009).
[12]Y. L. Chen, J. G. Analytis, J. H. Chu, Z. K. Liu, S. K. Mo, X. L. Qi, H. J. Zhang, D. H. Lu, X. Dai, Z. Fang, S. C. Zhang, I. R. Fisher, Z. Hussain, and Z. X. Shen, Science **325**, 178 (2009).
[13]D. Hsieh, Y. Xia, D. Qian, L. Wray, F. Meier, J. H. Dil, J. Osterwalder, L. Patthey, A. V. Fedorov, H. Lin, A. Bansil, D. Grauer, Y. S. Hor, R. J. Cava, and M. Z. Hasan, Phys. Rev. Lett. **103**, 146401 (2009).
[14]J. Seo, P. Roushan, H. Beidenkopf, Y. S. Hor, R. J. Cava, and A. Yazdani, Nature **466**, 343 (2010).
[15]L. Hao, P. Thalmeier, and T. K. Lee, Phys. Rev. B **84**, 235303 (2011); G. H. Liu, G. H. Zhou, and Y. H. Chen, Appl. Phys. Lett. **101**, 223109 (2012).
[16]S. Mondal, D. Sen, K. Sengupta, and R. Shankar, Phys. Rev. Lett. **104**, 046403 (2010).
[17]A. Narayan, I. Rungger, and S. Sanvito, New J. Phys. **17**, 033021 (2015).
[18]K. H. Zhang, Z. C. Wang, Q. R. Zheng, and G. Su, Phys. Rev. B **86**, 174416 (2012).
[19]Y. Zheng and T. Ando, Phys. Rev. B **65**, 245420 (2002).
[20]L. Fu and C. L. Kane, Phys. Rev. Lett. **100**, 096407 (2008).
[21]Z. Wu, F. M. Peeters, and K. Chang, Phys. Rev. B **82**, 115211 (2010).
[22]L. Feng, M. Ayache, J. Q. Huang, Y. L. Xu, M. H. Lu, Y. F. Chen, Y. Fainman, and A. Scherer, Science **333**, 729 (2011).
[23]Y. Zhou, Y. Q. Dong, K. Zhang, R. W. Peng, Q. Hu, and M. Wang, Europhys. Lett. **107**, 54001 (2014).
[24]A. Matulis, F. M. Peeters, and P. Vasilopoulos, Phys. Rev. Lett. **72**, 1518 (1994).
[25]J. Hong, S. Joo, T. Kim, K. Rhie, K. H. Kim, and S. U. Kim, Appl. Phys. Lett. **90**, 023510 (2007).
[26]L. Fu, Phys. Rev. Lett. **103**, 266801 (2009).
[27]Q. Li, E. Rossi, and S. D. Sarma, Phys. Rev. B **86**, 235443 (2012).
[28]D. Kim, S. Cho, N. P. Butch, P. Syers, K. Kirshenbaum, J. Paglione, and M. S. Fuhrer, Nat. Phys. **8**, 460 (2012).
[29]M. S. Bahramy, P. King, A. Torre, J. Chang, M. Shi, L. Patthey, G. Balakrishnan, P. Hofmann, R. Arita, N. Nagaosa, and F. Baumberger, Nat. Commun. **3**, 1159 (2012).
[30]C. H. Li, O. Erve, S. Rajput, L. Li, and B. T. Jonker, Nat. Commun. **7**, 13518 (2016).